Article

Iloprost requires the Frizzled-9 receptor to prevent lung cancer

Kayla Sompel, Lori D. Dwyer-Nield, Alex J. Smith, ..., Katrina Kopf, Robert L. Keith, Meredith A. Tennis

meredith.tennis@cuanschutz.edu

Highlights

Loss of Frizzled 9 reduces the lung cancer chemopreventive effect of iloprost in mice

Lung cancer prevention by prostacyclin synthase in mice does not require Frizzled 9

Activation of iloprost downstream targets is reduced with loss of Frizzled 9

Article

Iloprost requires the Frizzled-9 receptor to prevent lung cancer

Kayla Sompel,[1] Lori D. Dwyer-Nield,[2] Alex J. Smith,[1] Alamelu Elango,[1] Don S. Backos,[2] Bicheng Zhang,[3] James Gross,[3] Kristina Ternyak,[3] Jennifer L. Matsuda,[3] Katrina Kopf,[3] Robert L. Keith,[1,4] and Meredith A. Tennis[1,5,*]

SUMMARY

Prevention of premalignant lesion progression is a promising approach to reducing lung cancer burden in high-risk populations. Substantial preclinical and clinical evidence has demonstrated efficacy of the prostacyclin analogue iloprost for lung cancer chemoprevention. Iloprost activates peroxisome proliferator-activated receptor gamma (PPARG) to initiate chemopreventive signaling and *in vitro*, which requires the transmembrane receptor Frizzled$_9$ (FZD$_9$). We hypothesized a $Fzd_9^{-/-}$ mouse would not be protected by iloprost in a lung cancer model. $Fzd_9^{-/-}$ mice were treated with inhaled iloprost in a urethane model of lung adenoma. We found that $Fzd_9^{-/-}$ mice treated with iloprost were not protected from adenoma development compared to wild-type mice nor did they demonstrate increased activation of iloprost signaling pathways. Our results established that iloprost requires FZD$_9$ *in vivo* for lung cancer chemoprevention. This work represents a critical advancement in defining iloprost's chemopreventive mechanisms and identifies a potential response marker for future clinical trials.

INTRODUCTION

Iloprost is a prostacyclin analogue and an FDA approved pulmonary hypertension therapy that has been repurposed as a lung cancer chemoprevention agent (clinical trials: NCT00084409, NCT02237183). In the oral iloprost clinical trial, former smokers had reduced endobronchial dysplasia with six months of iloprost compared to placebo (Keith et al., 2011). Increased understanding of iloprost's mechanism of action is the key to moving this prevention strategy to the clinic for high-risk patients. Prostacyclins activate peroxisome proliferator- activated receptor gamma (PPARG) through the lone prostacyclin receptor IP and *PPARG* transgenic mice develop fewer lung tumors after urethane exposure compared to wild-type mice, an effect that is not enhanced by treatment with iloprost (Nemenoff et al., 2008). When *IP* null mice are crossed with lung epithelial cell-specific prostacyclin synthase overexpression ($Pgis^{Tg}$) mice, they are still protected from lung cancer (Nemenoff et al., 2008). Because an alternative to IP is involved in prostacyclin protection in these models, Frizzled$_9$ (FZD$_9$) was hypothesized to be involved because of its role in similar signaling through PPARG. FZD$_9$ is a seven-transmembrane domain G protein-coupled receptor that binds WNT7A in the lung and signals to PPARG, leading to normal lung epithelial maintenance (Winn et al., 2005, 2006). This contrasts with most WNT/FZD binding that activates oncogenic β-catenin signaling, where, for example, WNT signaling can enhance proliferation of *KRAS* mutant mouse adenocarcinoma cells or where blocking WNT signaling can cause apoptosis in squamous carcinoma cells (He et al., 2004; Pacheco-Pinedo et al., 2011). *WNT*s and *FZD*s are variably expressed across different NSCLC histology cell lines, but *FZD$_9$* is rarely expressed in these lines (Winn et al., 2005). *In vitro* experiments demonstrate that iloprost inhibits transformed growth of NSCLC cell lines, but *only* in cells with *FZD$_9$* expression (Tennis et al., 2010). Knockdown of *FZD$_9$* expression in NSCLC cells blocks response to iloprost and prevents activation of PPARG (Tennis et al., 2010). Of the ten FZDs, only FZD$_9$ activates PPARG with iloprost treatment, supporting a specific relationship between iloprost, FZD$_9$, and PPARG (Tennis et al., 2010).

In vitro and *in vivo* models have demonstrated downstream effects of iloprost on markers of epithelial to mesenchymal transition (EMT). Iloprost decreases expression of snail and vimentin and increases e-cadherin and crumbs3 in a human bronchial epithelial cell line, and mice with increased levels of prostacyclin have similar expression changes (New et al., 2018). Iloprost also alters EMT gene expression in cultured

[1]Division of Pulmonary Sciences and Critical Care Medicine, School of Medicine, University of Colorado Anschutz Medical Campus, Aurora, CO, USA

[2]Skaggs School of Pharmacy, University of Colorado Anschutz Medical Campus, Aurora, CO, USA

[3]National Jewish Health, Denver, CO, USA

[4]Rocky Mountain Regional VA Medical Center, Aurora, CO, USA

[5]Lead contact

*Correspondence: meredith.tennis@cuanschutz. edu

https://doi.org/10.1016/j.isci. 2022.104442

dysplastic cells (New et al., 2018). Both oral and inhaled iloprost reduce multiplicity of urethane-induced adenomas and inhaled iloprost affects expression of EMT genes (Nemenoff et al., 2008; Tennis et al., 2021). With preclinical and clinical evidence for effectiveness of iloprost against premalignant lung lesions, we aim to increase understanding of mechanisms of action and potential response markers for implementation of iloprost chemoprevention in high-risk patients. Here, we present data from an *in vivo* model of inhaled iloprost lung cancer chemoprevention with $Fzd_9^{-/-}$ mice confirming that FZD$_9$ is required for activity of iloprost and reduced adenoma multiplicity.

RESULTS

Loss of *Fzd₉* decreases intranasal iloprost efficacy *in vivo*

We previously identified both a dependence on FZD$_9$ signaling for iloprost activity and a decrease in FZD_9 expression following cigarette smoke exposure in a human cultured lung epithelial cell line (Tennis et al., 2010, 2016). We generated the first FVBN $Fzd_9^{-/-}$ mouse using a CRISPR approach in collaboration with the Regional Mouse Genetics Core Facility at National Jewish Health (manuscript under review). After sequence confirmed knockout, animals were bred and genotyped to confirm transmission of the knockout to subsequent generations. To further analyze the effect of Fzd_9 expression on iloprost chemoprevention treatment, $Fzd_9^{-/-}$ mice and wild-type (WT) mice were administered a single dose of urethane and after 9 weeks, treated with intranasal iloprost 5 days/week for 6 weeks (Figure 1A). After 15 weeks, no group of mice had a significant difference in weight (Figure 1B). WT mice treated with intranasal iloprost in this study had a 50% decrease in adenoma multiplicity compared to the wild-type control group (Figure 1C) (though not significant in this experiment (p = 0.09), this has been previously reported as significant) (Nemenoff et al., 2008; Tennis et al., 2021). In contrast, $Fzd_9^{-/-}$ mice treated with Iloprost had a slightly increased number of adenomas compared to $Fzd_9^{-/-}$ saline controls (Figure 1C). $Fzd_9^{-/-}$ iloprost-treated mice had a significant increase of 130% more adenomas compared to WT iloprost-treated mice (Figure 1C). There were no differences in adenoma diameter (Figure 1D). The effect of iloprost on adenoma proliferation state in each group was determined by Ki67 immunohistochemistry. Relative to their genotype saline treated controls, WT urethane mice had a larger decrease in Ki67 expression with iloprost treatment than $Fzd_9^{-/-}$ urethane mice with iloprost treatment (Figure 1E, see also Table S1). However, these data represent only a trend, as statistical analysis could not be completed on the entire group because although three samples were collected for Ki67 staining from each group, only one WUI section had a lesion, likely because of the preventive effects of iloprost. Figure 1F shows a microCT image and Figure 1G shows an H&E stain representative of adenoma development in the 14-week urethane model in the FVB strain. Decreased lesion multiplicity and a trend toward decreased Ki67 expression demonstrate that the chemopreventive activity of iloprost is reduced with loss of Fzd_9 expression *in vivo*.

Prostacyclin does not require *Fzd₉* for protective effects

Preclinical lung cancer prevention studies using FVBN prostacyclin synthase transgenic mice ($Pgis^{Tg}$), demonstrated that increased prostacyclin reduces lung adenoma formation *in vivo*, but this does not require the traditional prostacyclin receptor IP (Keith et al., 2002, 2004; Nemenoff et al., 2008). We found that iloprost requires Fzd_9 for anticancer signaling *in vitro* and *in vivo*, so we were interested in whether Fzd_9 was required for the *in vivo* protection seen in Pgis^{Tg} mice. We crossed $Pgis^{Tg}$ mice with $Fzd_9^{-/-}$ mice to generate $Pgis^{Tg}xFzd_9^{-/-}$ mice, confirmed $Pgis^{Tg}$ and $Fzd_9^{-/-}$ by genotyping, and used these mice in the urethane model of lung adenomas (Figure 2A). After 16 weeks, $Pgis^{Tg}xFzd_9^{-/-}$ urethane mice had statistically significant lower weight than the WT urethane mice (p = 0.03), but there was no difference in weight compared to $Pgis^{Tg}$ urethane mice (Figure 2B). The $Pgis^{Tg}xFzd_9^{-/-}$ mice had no other indications of poor health upon evaluation by the facility veterinarian. Saline mice had no weight differences and no adenomas. Average adenoma multiplicity per group 16 weeks after urethane exposure was decreased in $Pgis^{Tg}$ mice compared to WT mice, but there was no difference between $Pgis^{Tg}$ ^{g} and $Pgis^{Tg}xFzd_9^{-/-}$ (Figure 2C). Adenoma size was significantly different between WT and $Pgis^{Tg}$ mice, but not different between $Pgis^{Tg}xFzd_9^{-/-}$ and other groups (Figure 2C). Prostacyclin protection from lung adenomas does not appear to rely on Fzd_9 expression; however, the study was limited by lower-than-expected overall lesion numbers with urethane exposure.

Loss of *Fzd₉* reverses the effect of iloprost on downstream target expression and activity

Prostacyclin reverses EMT gene expression and downstream targets of PPARG in the lung *in vitro* and *in vivo*, so we measured expression changes in these genes in the $Fzd_9^{-/-}$ urethane/iloprost mouse study (New et al., 2018). Adenomas from urethane exposed WT and $Fzd_9^{-/-}$ mice were dissected from lung tissue
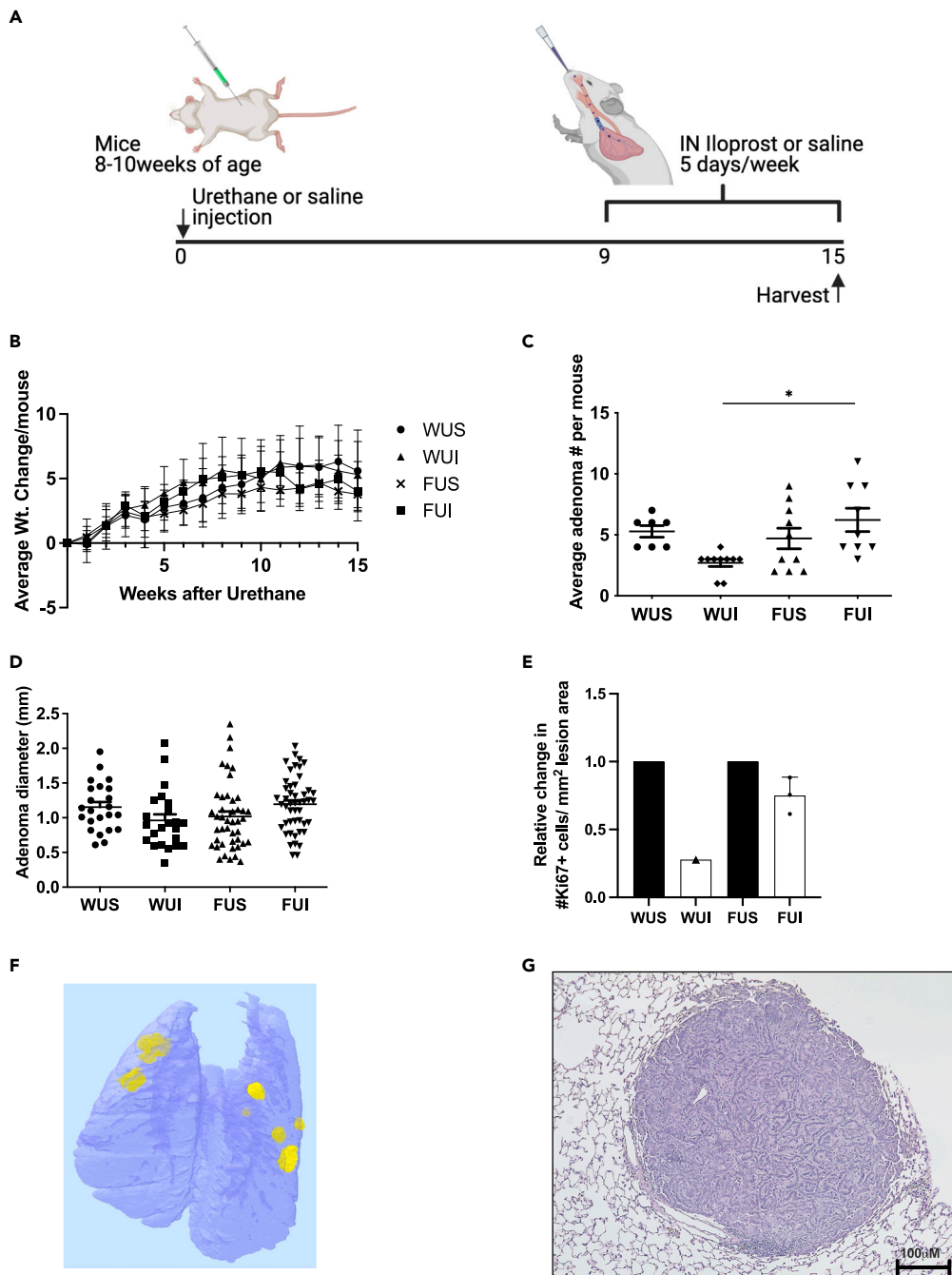
Figure 1. Iloprost requires _Fzd9_ to prevent murine adenoma development

(A) Schematic of urethane and inhaled iloprost lung cancer chemoprevention model.

(B) Change in weights of mice in the urethane and inhaled iloprost model.

(C) Average adenoma number per mouse in the urethane exposed groups.

(D) Diameter of adenomas in urethane exposed groups.

(E) Average number of Ki67 expressing cells/mm^2 adenoma area per mouse exposed to urethane. Urethane mice are compared to their genotype saline control.

(F) microCT image of _Fzd9_$^{-/-}$ urethane iloprost mouse lung.

(G) H&E of a representative adenoma generated by the 15-week urethane model. WUS, wild type urethane saline; WUI, wild type urethane iloprost; FUS, _Fzd9_$^{-/-}$ urethane saline; FUI, _Fzd9_$^{-/-}$ urethane iloprost. Data are represented as mean ± SEM. One-way ANOVA with Tukey's post hoc test was used to measure significance. *p < 0.05. Scale bar is 100uM.
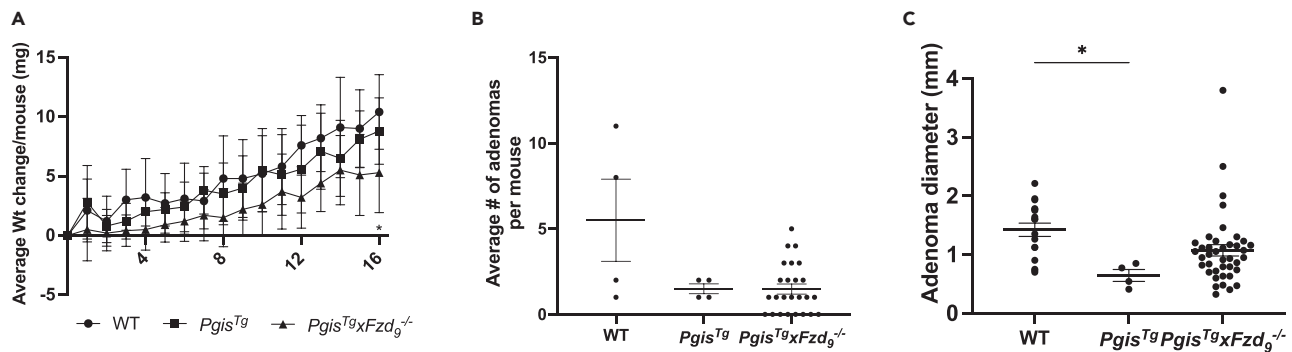
Figure 2. Transgenic prostacyclin does not require *Fzd₉* expression for preventive effects in the mouse lung

(A) Change in weights of mice in the urethane model.

(B) Average adenoma number per mouse in the urethane exposed groups.

(C) Diameter of adenomas in urethane exposed groups. WT, wild type; $Pgis^{Tg}$, prostacyclin synthase transgenic; $Pgis^{Tg}$ x $Fzd_9^{-/-}$ prostacyclin synthase transgenic with Fzd_9 knockout. Data are represented as mean ± SEM. A one-way ANOVA with Tukey's post-hoc test was used to measure significance. *$p < 0.05$.

and analyzed by qPCR. In WT mice exposed to urethane, iloprost treatment led to higher levels of prostacyclin targets carboxylesterase 1 (*Ces1*), *Pparg*, and epithelial marker crumbs3 (*Crb3*) compared to urethane exposed saline controls (Figure 3A). WT urethane iloprost mice also expressed lower levels of lung tumor-associated genes vascular endothelial growth factor (*Vegf*) and estrogen receptor 1 (*Esr1*) compared to saline treated controls (Figure 3A). In contrast, in $Fzd_9^{-/-}$ mice exposed to urethane, iloprost treatment led to adenomas with lower *Ces1*, *Pparg*, and *Crb3* and higher *Vegf* and *Esr1* compared to saline controls (Figure 3A). A similar trend was observed in whole lung tissue from the same mice. In lungs from WT urethane exposed mice, iloprost increased expression of e-cadherin (*Ecad*), *Ces1*, and prostacyclin target *15-pgdh* and decreased expression of vimentin (*Vim*) (Figure 3B). In lungs from $Fzd_9^{-/-}$ mice, iloprost had no significant effect on these genes (Figure 3B). Protein expression by western blot in $Fzd_9^{-/-}$ urethane mice had less e-cadherin (ECAD) than WT urethane mice and no increase with iloprost treatment (Figures 3C and 3D, see also Figure S3). COX2 protein, which is decreased by PPARG signaling in the lung, was higher in $Fzd_9^{-/-}$ urethane mice compared to WT urethane mice (Figures 3C and 3D). COX2 expression decreased slightly in WT urethane mice after iloprost treatment but increased in $Fzd_9^{-/-}$ urethane mice treated with iloprost (Figures 3C and 3D). These alterations in downstream targets support the hypothesis that $Fzd_9^{-/-}$ loss rescues iloprost chemopreventive activity.

To investigate whether loss of Fzd_9 expression influences iloprost's activation of PPARG, serum collected from WT and $Fzd_9^{-/-}$ mice was added to 293T cells and its effect on a peroxisome proliferator-activated receptor gamma (PPRE) luciferase was analyzed by dual luciferase reporter assay (Edwards et al., 2019). Serum from WT urethane mice treated with iloprost stimulated significantly higher PPRE activity than the WT urethane saline treated group (Figure 4). There was no difference between the $Fzd_9^{-/-}$ urethane iloprost and urethane saline groups (Figure 4). This demonstrates that loss of Fzd_9 prevents the activation of PPARG that is characteristic of iloprost chemoprevention.

FZD₉ is a potential receptor for iloprost

The prostacyclin receptors are seven transmembrane spanning receptors; similar to FZD₉ and the prostacyclin receptor, IP is not required for the preventive effects of prostacyclin or iloprost in the lung, suggesting an alternative receptor may mediate iloprost's effects. We are interested in whether iloprost can bind to FZD₉, so we performed computational-based molecular modeling studies to predict the binding mode of iloprost in FZD₉. Small molecule docking studies indicated that iloprost has a good potential to bind the ligand binding pocket of FZD₉ by virtue of extensive favorable contact between the carboxylic acid moiety and residue Y277 at the bottom of the pocket. This includes strong electrostatic and hydrogen bond interactions, as well as hydrophobic interactions involving the ring system (Figure S5A). Indeed, all of the top scoring poses in the docking results occupied the same region of the protein and presented a similar interaction pattern. The solvent-corrected binding energy of the presented iloprost binding mode was −8.9 kcal/mol, likewise indicating the overall binding favorability. Based on these potential interactions,
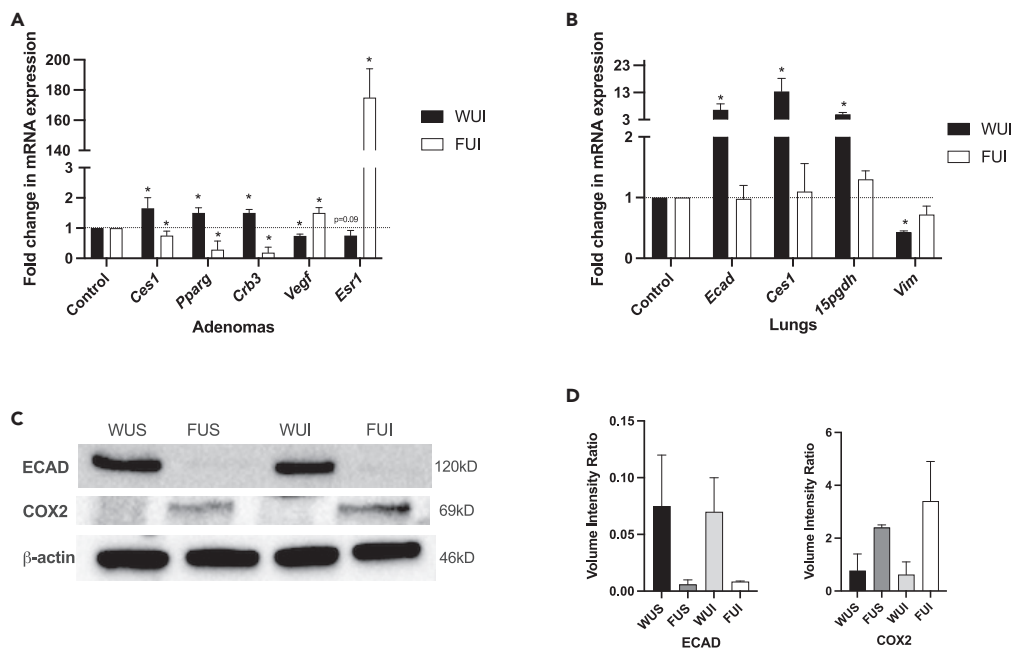
Figure 3. Loss of *Fzd₉* *in vivo* prevents iloprost-induced expression changes

(A) mRNA expression in adenomas from urethane exposed WT and *Fzd₉⁻/⁻* mice treated with iloprost or saline control.

(B) Whole lung mRNA expression from the same mice. PCR expression was normalized to *RPS18*, and relative change and p-value calculated relative to each genotype's urethane/saline control. Data are represented as mean ± SEM. Student's *t*-tests were used to measure significance. *p < 0.05.

(C) Western blots of mouse whole lung tissue for ECAD, COX2, and β-actin loading control (see Figure S4 for full blot).

(D) Quantification of western blot band density (N = 2). Data are represented as mean ± SEM. A one-way ANOVA with Tukey's post hoc test was used to measure significance. *p < 0.05 WUS, wild type urethane saline; WUI, wild type urethane iloprost; FUS, *Fzd₉⁻/⁻* urethane saline; FUI, *Fzd₉⁻/⁻*, urethane iloprost.

a plasmid was generated by site-directed mutagenesis with a point mutation leading to an amino acid substitution—Y277S—in the FZD₉ binding pocket (Figure S5B). A549 (adenocarcinoma) and Human Bronchial Epithelial Cells (HBEC) cell lines were transfected with the mutant plasmid, and its effect on iloprost activity was evaluated using PPRE luciferase, a measure of downstream iloprost signaling. Both FZD₉ and iloprost activate PPRE luciferase, and this is used as a readout of downstream activity (Smith et al., 2022; Tennis et al., 2010, 2016). Following two 10uM iloprost doses, PPRE luciferase activity increased in both A549 and HBEC cell lines. When iloprost was combined with transfection of the mutant plasmid, PPRE activity did not increase in either cell line, suggesting that the *Fzd₉* mutant plasmid may prevent iloprost signaling (Figures S5C and S5D). This supports further investigation into whether iloprost functions as a FZD₉ ligand and activator of FZD₉ downstream signaling.

DISCUSSION

Iloprost is an FDA approved drug that was repurposed for lung cancer chemoprevention and has positive clinical trial results with minimal side effects (Keith et al., 2011). Previous *in vitro* work demonstrated that iloprost requires *FZD₉* expression to activate PPARG cancer preventive signaling (Tennis et al., 2010). Our current study presents the critical finding that *in vivo*, the chemopreventive effect of iloprost on pulmonary adenomas is dependent on *Fzd₉* expression. To investigate the role of FZD₉ in iloprost activity, we compared wild type and *Fzd₉⁻/⁻* mice with exposure to urethane and treatment with intranasal iloprost. Iloprost decreased adenoma burden in wild type mice, whereas no significant difference was observed in *Fzd₉⁻/⁻* mice treated with iloprost. We also compared adenomas from wild type and *Fzd₉⁻/⁻* iloprost-treated mice and saw no change in proliferation by Ki67 staining, suggesting that Fzd₉ is important for an effect of iloprost on proliferation. However, no change in adenoma size with iloprost in our study suggests that inhibition of proliferation may not be the main effect of iloprost, which is supported by data from a clinical trial of iloprost lung cancer chemoprevention that found only a nonsignificant decreased in Ki67
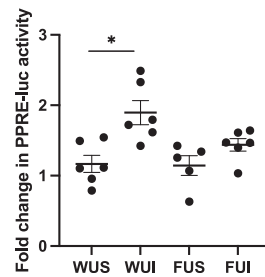
Figure 4. Loss of *Fzd₉* *in vivo* reduces active PPARG in serum

Serum was collected from wild type urethane saline (WUS), wildtype urethane iloprost (WUI), $Fzd_9^{-/-}$ urethane saline (FUS), and $Fzd_9^{-/-}$ urethane iloprost (FUI) mice. 293t cells were transfected with PPRE and mouse serum was added to the media, followed by luciferase measurement at 48 h (N = 3). Fold change is relative to a luciferase control. Data are represented as mean ± SEM. One-way ANOVA with Tukey's post hoc test was used to measure significance. *p < 0.05.

staining (Keith et al., 2011). Expression and activity data demonstrate that iloprost decreases proliferation and EMT in lesions but is not effective without the presence of Fzd_9. Studies using the $Pgis^{Tg}$ mouse in lung cancer models have demonstrated the chemoprotective effect of endogenously produced prostacyclin; however, our results demonstrated that Fzd_9 is not required for this effect. This suggests that the relevance of FZD₉ for prostacyclin chemoprevention is limited to iloprost. If prostacyclin does not require its traditional receptor IP or FZD₉ to exert chemoprotective effects, there must be alternative receptors or pathways that stimulate preventive signaling with prostacyclin binding (Whittle et al., 2012). Additional studies will be required to investigate the protective mechanisms of prostacyclin overexpression.

Differences in preventive pathway signaling component expression after iloprost treatment confirm the importance of FZD₉ for activation or suppression of iloprost targets. Changes in EMT are associated with early lesion development in the lung and EMT is often a target of chemopreventive agents (New et al., 2018; Tennis et al., 2016; Jaromy and Miller, 2021; Liu et al., 2019). Reversal of EMT gene expression is associated with iloprost treatment *in vitro* and *in vivo* (New et al., 2018). In the whole lung, we found expression of epithelial genes increased, and expression of mesenchymal genes decreased in iloprost-treated wild-type mice but not in $Fzd_9^{-/-}$ mice. In adenomas, epithelial marker *Crb3* was upregulated with iloprost in wild-type mice but not in $Fzd_9^{-/-}$ mice. *Ces1* and *Pparg*, which are associated with activation of prostacyclin signaling in the lung, were not increased in adenomas from $Fzd_9^{-/-}$ mice after iloprost (New et al., 2018; Keith et al., 2004). *Ces1* also increased in whole lung tissue from wild-type mice treated with iloprost but not $Fzd_9^{-/-}$ mice. *15pgdh*, a tumor suppressive enzyme that inactivates prostaglandin E2 (PGE2) and is increased by PPARG activation, was increased with iloprost in wild-type mice but not in $Fzd_9^{-/-}$ mice (Kim et al., 2015). The decrease observed in COX2 protein in the whole lung between wild type control and wild type iloprost, though minimal, suggests that iloprost may alter inflammatory signaling. Increased COX2 in $Fzd_9^{-/-}$ iloprost-treated mice indicates that, without Fzd_9, iloprost may activate an alternative pathway that increases inflammatory signals. Decreased inflammatory signaling in biopsies of squamous lung dysplasia is associated with high-grade lesion persistence, suggesting a conflict between the ability of iloprost to reduce high-grade lesions and its potential anti-inflammatory role (Keith et al., 2011; Merrick et al., 2018). Further work will need to delineate the context and timing of effects of iloprost on inflammation during the progression of premalignant lung lesions.

Vegf, which is associated with reduced survival in lung adenocarcinoma patients, was decreased in adenomas with iloprost in wild type mice but increased in $Fzd_9^{-/-}$ iloprost-treated mice (Jung et al., 2021; Naikoo et al., 2017). Although *Esr2* is predominantly expressed in lung tissue and lung tumors, we only detected changes in *Esr1* in adenomas from our mouse model (Liau et al., 2021). *Esr1* was decreased in adenomas from wild-type mice treated with iloprost but significantly elevated in adenomas from $Fzd_9^{-/-}$ mice treated with iloprost. The increased expression of *Vegf* and *Esr1* with iloprost treatment in $Fzd_9^{-/-}$ mice suggests that tumor promoting signals may be caused by the combination of iloprost and Fzd_9 loss. Without Fzd_9, iloprost may target other receptors that do not stimulate chemopreventive signaling but promote lesion development. We observed a small but nonsignificant increase in adenomas after urethane with iloprost treatment in $Fzd_9^{-/-}$ mice compared to $Fzd_9^{-/-}$ saline treated mice, suggesting that a larger or longer study may have detected increased lesion number in $Fzd_9^{-/-}$ mice treated with iloprost. Overall, these expression changes paint a picture of iloprost's reduced capacity to activate protective signaling pathways in the lung epithelium and the potential for tumor promotion without the presence of Fzd_9.

Efficacy of iloprost was measured in the oral and inhaled iloprost clinical trials by bronchoscopy with biopsy at baseline and follow up. This method identifies histologic changes in lung cells and the presence of persistent dysplasia detected by bronchoscopy is associated with increased risk of developing squamous carcinoma (Merrick et al., 2016). Additional measures of iloprost response are needed to bring iloprost chemoprevention to the clinic, especially noninvasive molecular tests. Edwards et al. recently described an assay that measured the activation of PPARG in mouse and human serum (Edwards et al., 2019). We used this assay to measure activity of PPARG in serum samples from animals in our study. This experiment verified that the activation of PPARG was decreased in $Fzd_9^{-/-}$ mice treated with iloprost compared to wild-type mice treated with iloprost. If PPARG activation can be correlated with histologic response to iloprost, this assay could inform a potential noninvasive response test for future clinical applications of iloprost. This type of assay could allow providers to monitor patients receiving iloprost chemoprevention at multiple time points to determine if they should continue treatment, reducing the potential for side effects in patients who are not benefiting from the intervention.

A greater understanding of the mechanism of activity for iloprost chemoprevention will speed its clinical application. Studies have demonstrated that FZD_9 is required for iloprost activity; however, it is still unknown if they interact directly. The concept that FZDs could be direct targets for small molecule drugs has been challenged in the past. Recently, however, smoothened agonist SAG1.3 was shown to bind FZD_6 to induce conformational changes in the receptor and stimulate activation and interactions in the FZD_6 signaling pathway (Kozielewicz et al., 2020). This work supports our interest in defining the specific relationship between FZD_9 and iloprost and suggests opportunities to target FZDs in cancer (Sompel et al., 2021). No crystal structure of FZD_9 exists, but by using structures of homologous proteins, we generated an *in silico* molecular model for iloprost and FZD_9 interaction that suggested favorable structures for binding. With knowledge of specific residues in the FZD_9 binding pocket that might influence iloprost binding, we mutated FZD_9 at a single residue. This mutation in the potential binding pocket decreased iloprost's ability to activate PPARG, suggesting interaction with FZD_9 may be required for iloprost's chemopreventive function. These data support further investigation of the hypothesis that iloprost agonizes FZD_9 and encourages additional *in vitro* and structural studies to explore this critical piece of iloprost's mechanism.

In summary, substantial *in vitro* and now *in vivo* data support the essential role of FZD_9 in the activity of iloprost in lung epithelium, adding to our understanding of iloprost's chemopreventive mechanisms. Because it is required for iloprost activity, FZD_9 expression may be a mechanistically relevant marker for predicting response to iloprost. Further testing of our *ex vivo* PPARG activity assay may provide the first noninvasive measure of iloprost activity in patients. Chemoprevention is an essential tool for reducing the burden of cancer in high-risk populations and this study adds to mounting evidence for the use of iloprost as lung cancer chemoprevention in former smokers and suggests new directions for future research.

Limitations of the study

Models using chemical carcinogens to induce cancer in mice are essential for chemoprevention studies but do have some challenges. Experimental groups often have expected but unpredictable death, which can lead to uneven group sizes to include all surviving animals in final analyses. We can try to compensate for this with larger group sizes for mice with unknown reactions to new treatments. We included larger groups for the $Fzd_9^{-/-}$ mice, because the combination of urethane and iloprost was untested in this genotype and we wanted to ensure sufficient animals survived for statistical analysis of lesion numbers. Urethane in wild-type animals has been tested repeatedly, so we could use smaller numbers for control animals, which is important for addressing the three R's of animal research. Also because of unpredictability in carcinogen models, the wild type iloprost group in this study had a nonsignificant decrease in adenoma multiplicity (p = 0.09). Reduced premalignant lesions with iloprost treatment have achieved statistical significance in previous studies (Tennis et al., 2021; Nemenoff et al., 2008). For proliferation analysis of adenomas with Ki67 staining, we collected our standard of three fixed specimens per group, but statistical analysis was limited by the presence of a lesion in only one of the wild type urethane iloprost lungs selected for fixation. With no crystal structure of FZD_9 available for our *in silico* binding analysis, we had to use structures of homologous proteins to generate a molecular model for a possible iloprost and FZD_9 interaction (Figure S5A). The utility of existing structures of other FZDs is limited because of low-resolution and unsuitability for docking analysis, so using the SMO structure is the best approach at this time.

STAR★METHODS

Detailed methods are provided in the online version of this paper and include the following:

- KEY RESOURCES TABLE
- RESOURCE AVAILABILITY
  - Lead contact
  - Materials availability
  - Data and code availability
- EXPERIMENTAL MODEL AND SUBJECT DETAILS
  - Animals: Mice
  - Mouse genotyping
  - $Fzd_9{}^{-/-}$ inhaled iloprost *in vivo* study
  - $Pgis^{Tg}$ x $Fzd_9{}^{-/-}$ urethane *in vivo* study
  - Cells
- METHOD DETAILS
  - MicroCT imaging
  - Reverse transcriptase-quantitative PCR
  - Western blots
  - Immunohistochemistry
  - Serum PPARG activity assay
  - *In silico* binding prediction
  - Mutant plasmid transfections
- QUANTIFICATION AND STATISTICAL ANALYSIS
  - $Fzd_9{}^{-/-}$ adenoma counts
  - $Pgis^{Tg}$x $Fzd_9{}^{-/-}$ adenoma counts
  - Adenoma diameter measurements
  - Average weight change in mouse studies
  - Reverse transcriptase-quantitative PCR
  - Western Blot quantitative analysis
  - Ki67 proliferative index
  - Serum PPARG activity assay
  - Site directed mutagenesis

SUPPLEMENTAL INFORMATION

Supplemental information can be found online at https://doi.org/10.1016/j.isci.2022.104442.

AUTHOR CONTRIBUTIONS

Conceptualization, M.T., L.N., and R.K.; Methodology, J.S., B.Z., J.G., K.T., and K.K.; Investigation, K.S., A.S., A.E., L.N., and D.S.; Funding Acquisition, M.T.; Project Administration, K.S., E.A., and M.T.; Supervision, M.T. and L.N.; Writing – Original Draft, KS and MT.; Writing – Review & Editing, K.S., E.A., M.T., L.N., R.K., and D.S.

DECLARATION OF INTERESTS

The authors declare no competing interests.

REFERENCES

Dwyer-Nield, L., Hickey, G.A., Friedman, M., Choo, K., Mcarthur, D.G., Tennis, M.A., New, M.L., Geraci, M., and Keith, R.L. (2017). The second-generation PGI2 analogue treprostinil fails to chemoprevent tumors in a murine lung adenocarcinoma model. Cancer Prev. Res. *10*, 671–679. https://doi.org/10.1158/1940-6207.capr-17-0050.

Edwards, L., Watt, J., Webster, T.F., and Schlezinger, J.J. (2019). Assessment of total, ligand-induced peroxisome proliferator activated receptor gamma ligand activity in serum. Environ. Health *18*, 45. https://doi.org/10.1186/s12940-019-0486-2.

Feig, M., Onufriev, A., Lee, M.S., Im, W., Case, D.A., and Brooks, C.L.,3R.D. (2004). Performance comparison of generalized born and Poisson methods in the calculation of electrostatic solvation energies for protein structures. J. Comput. Chem. *25*, 265–284. https://doi.org/10.1002/jcc.10378.

Fritz, J.M., Tennis, M.A., Orlicky, D.J., Lin, H., Ju, C., Redente, E.F., Choo, K.S., Staab, T.A., Bouchard, R.J., Merrick, D.T., et al. (2014). Depletion of tumor-associated macrophages slows the growth of chemically induced mouse lung adenocarcinomas. Front. Immunol. *5*, 587. https://doi.org/10.3389/fimmu.2014.00587.

He, B., You, L., Uematsu, K., Xu, Z., Lee, A.Y., Matsangou, M., Mccormick, F., and Jablons, D.M. (2004). A monoclonal antibody against Wnt-1 induces apoptosis in human cancer cells. Neoplasia *6*, 7–14. https://doi.org/10.1016/s1476-5586(04)80048-4.

Hooft, R.W.W., Vriend, G., Sander, C., and Abola, E.E. (1996). Errors in protein structures. Nature *381*, 272. https://doi.org/10.1038/381272a0.

Jaromy, M., and Miller, J.D. (2021). Pharmacologic mechanisms underlying antidiabetic drug metformin's chemopreventive effect against colorectal cancer. Eur. J. Pharmacol. *897*, 173956. https://doi.org/10.1016/j.ejphar.2021.173956.

Jung, W.Y., Min, K.W., and Oh, Y.H. (2021). Increased VEGF-A in solid type of lung adeno-carcinoma reduces the patients' survival. Sci. Rep. *11*, 1321. https://doi.org/10.1038/s41598-020-79907-6.

Keith, R.L., Blatchford, P.J., Kittelson, J., Minna, J.D., Kelly, K., Massion, P.P., Franklin, W.A., Mao, J., Wilson, D.O., Merrick, D.T., et al. (2011). Oral iloprost improves endobronchial dysplasia in former smokers. Cancer Prev. Res. *4*, 793–802. https://doi.org/10.1158/1940-6207.capr-11-0057.

Keith, R.L., Miller, Y.E., Hoshikawa, Y., Moore, M.D., Gesell, T.L., Gao, B., Malkinson, A.M., Golpon, H.A., Nemenoff, R.A., and Geraci, M.W. (2002). Manipulation of pulmonary prostacyclin synthase expression prevents murine lung cancer. Cancer Res. *62*, 734–740.

Keith, R.L., Miller, Y.E., Hudish, T.M., Girod, C.E., Sotto-Santiago, S., Franklin, W.A., Nemenoff, R.A., March, T.H., Nana-Sinkam, S.P., and Geraci, M.W. (2004). Pulmonary prostacyclin synthase overexpression chemoprevents tobacco smoke lung carcinogenesis in mice. Cancer Res. *64*,

5897–5904. https://doi.org/10.1158/0008-5472.can-04-1070.

Kim, J., Sato, M., Choi, J.W., Kim, H.W., Yeh, B.I., Larsen, J.E., Minna, J.D., Cha, J.H., and Jeong, Y. (2015). Nuclear receptor expression and function in human lung cancer pathogenesis. PLoS One *10*, e0134842. https://doi.org/10.1371/journal.pone.0134842.

Koska, J., Spassov, V.Z., Maynard, A.J., Yan, L., Austin, N., Flook, P.K., and Venkatachalam, C.M. (2008). Fully automated molecular mechanics based induced fit protein-ligand docking method. J. Chem. Inf. Model. *48*, 1965–1973. https://doi.org/10.1021/ci800081s.

Kozielewicz, P., Turku, A., Bowin, C.F., Petersen, J., Valnohova, J., Canizal, M.C.A., Ono, Y., Inoue, A., Hoffmann, C., and Schulte, G. (2020). Structural insight into small molecule action on Frizzleds. Nat. Commun. *11*, 414. https://doi.org/10.1038/s41467-019-14149-3.

Krieger, E., Joo, K., Lee, J., Lee, J., Raman, S., Thompson, J., Tyka, M., Baker, D., and Karplus, K. (2009). Improving physical realism, stereochemistry, and side-chain accuracy in homology modeling: four approaches that performed well in CASP8. Proteins *77* (Suppl 9), 114–122. https://doi.org/10.1002/prot.22570.

Krieger, E., Koraimann, G., and Vriend, G. (2002). Increasing the precision of comparative models with YASARA NOVA–a self-parameterizing force field. Proteins *47*, 393–402. https://doi.org/10.1002/prot.10104.

Lammi, M.R., Ghonim, M.A., Pyakurel, K., Naura, A.S., Ibba, S.V., Davis, C.J., Okpechi, S.C., Happel, K.I., Deboisblanc, B.P., Shellito, J., and Boulares, A.H. (2016). Treatment with intranasal iloprost reduces disease manifestations in a murine model of previously established COPD. Am. J. Physiol. Lung Cell Mol. Physiol. *310*, L630–L638. https://doi.org/10.1152/ajplung.00297.2015.

Liau, C.S., Mogan, P., and Thomas, W. (2021). Oestrogen actions contribute to female gender-specific risks in the development of lung carcinoma. J. Steroid Biochem. Mol. Biol. *208*, 105786. https://doi.org/10.1016/j.jsbmb.2020.105786.

Liu, X., Wu, Y., Zhou, Z., Huang, M., Deng, W., Wang, Y., Zhou, X., Chen, L., Li, Y., Zeng, T., et al. (2019). Celecoxib inhibits the epithelial-to-mesenchymal transition in bladder cancer via the miRNA-145/TGFBR2/Smad3 axis. Int. J. Mol. Med. *44*, 683–693. https://doi.org/10.3892/ijmm.2019.4241.

Merrick, D.T., Edwards, M.G., Franklin, W.A., Sugita, M., Keith, R.L., Miller, Y.E., Friedman, M.B., Dwyer-Nield, L.D., Tennis, M.A., O'keefe, M.C., et al. (2018). Altered cell-cycle control, inflammation and adhesion in high-risk persistent bronchial dysplasia. Cancer Res. *78*, 4971–4983. https://doi.org/10.1158/0008-5472.can-17-3822.

Merrick, D.T., Gao, D., Miller, Y.E., Keith, R.L., Baron, A.E., Feser, W., Kennedy, T.C., Blatchford, P.J., Braudrick, S., Hirsch, F.R., et al. (2016). Persistence of bronchial dysplasia is associated with development of invasive squamous cell

carcinoma. Cancer Prev. Res. *9*, 96–104. https://doi.org/10.1158/1940-6207.capr-15-0305.

Naikoo, N.A., Dil, A., Rasool, R., Shah, S., Ahangar, A.G., Siddiqi, M.A., and Shah, Z.A. (2017). Upregulation of vascular endothelial growth factor (VEGF), its role in progression and prognosis of non-small cell lung carcinoma. Cancer Genet. *216–217*, 67–73. https://doi.org/10.1016/j.cancergen.2017.07.005.

Nemenoff, R., Meyer, A.M., Hudish, T.M., Mozer, A.B., Snee, A., Narumiya, S., Stearman, R.S., Winn, R.A., Weiser-Evans, M., Geraci, M.W., and Keith, R.L. (2008). Prostacyclin prevents murine lung cancer independent of the membrane receptor by activation of peroxisomal proliferator–activated receptor γ. Cancer Prev. Res. *1*, 349–356. https://doi.org/10.1158/1940-6207.capr-08-0145.

New, M.L., White, C.M., Mcgonigle, P., Mcarthur, D.G., Dwyer-Nield, L.D., Merrick, D.T., Keith, R.L., and Tennis, M.A. (2018). Prostacyclin and EMT pathway markers for monitoring response to lung cancer chemoprevention. Cancer Prev. Res. *11*, 643–654. https://doi.org/10.1158/1940-6207.capr-18-0052.

Pacheco-Pinedo, E.C., Durham, A.C., Stewart, K.M., Goss, A.M., Lu, M.M., Demayo, F.J., and Morrisey, E.E. (2011). Wnt/β-catenin signaling accelerates mouse lung tumorigenesis by imposing an embryonic distal progenitor phenotype on lung epithelium. J. Clin. Invest. *121*, 1935–1945. https://doi.org/10.1172/jci44871.

Smith, A.J., Do, P., Sompel, K., Elango, A., and Tennis, M.A. (2022). miR-520a-5p regulates Frizzled 9 expression and mediates effects of cigarette smoke and iloprost chemoprevention. Sci. Rep. *12*, 2388. https://doi.org/10.1038/s41598-022-06292-7.

Sompel, K.,E.A., Elango, A., Smith, A.J., and Tennis, M.A. (2021). Cancer chemoprevention through Frizzled receptors and EMT. Discover Oncol. *12*, 32. https://doi.org/10.1007/s12672-021-00429-2.

Tennis, M.A., New, M.L., Mcarthur, D.G., Merrick, D.T., Dwyer-Nield, L.D., and Keith, R.L. (2016). Prostacyclin reverses the cigarette smoke-induced decrease in pulmonary Frizzled 9 expression through miR-31. Sci. Rep. *6*, 28519. https://doi.org/10.1038/srep28519.

Tennis, M.A., Smith, A.J., Dwyer-Nield, L.D., and Keith, R.L. (2021). Intranasal iloprost prevents tumors in a murine lung carcinogenesis model. Cancer Prev. Res. *15*, 11–16. https://doi.org/10.1158/1940-6207.capr-21-0086.

Tennis, M.A., Van Scoyk, M., Heasley, L.E., Vandervest, K., Weiser-Evans, M., Freeman, S., Keith, R.L., Simpson, P., Nemenoff, R.A., and Winn, R.A. (2010). Prostacyclin inhibits non-small cell lung cancer growth by a frizzled 9-dependent pathway that is blocked by secreted frizzled-related protein 1. Neoplasia *12*, 244–253. https://doi.org/10.1593/neo.91690.

Vriend, G. (1990). What IF: a molecular modeling and drug design program. J. Mol. Graph. *8*, 52–56. https://doi.org/10.1016/0263-7855(90)80070-v.

Wang, C., Wu, H., Katritch, V., Han, G.W., Huang, X.P., Liu, W., Siu, F.Y., Roth, B.L., Cherezov, V., and Stevens, R.C. (2013). Structure of the human smoothened receptor bound to an antitumour agent. Nature *497*, 338–343. https://doi.org/10.1038/nature12167.

Whittle, B.J., Silverstein, A.M., Mottola, D.M., and Clapp, L.H. (2012). Binding and activity of the prostacyclin receptor (IP) agonists, treprostinil and iloprost, at human prostanoid receptors:

treprostinil is a potent DP1 and EP2 agonist. Biochem. Pharmacol. *84*, 68–75. https://doi.org/10.1016/j.bcp.2012.03.012.

Winn, R.A., Marek, L., Han, S.Y., Rodriguez, K., Rodriguez, N., Hammond, M., Van Scoyk, M., Acosta, H., Mirus, J., Barry, N., et al. (2005). Restoration of Wnt-7a expression reverses non-small cell lung cancer cellular transformation through frizzled-9-mediated growth inhibition and promotion of cell differentiation. J. Biol.

Chem. *280*, 19625–19634. https://doi.org/10.1074/jbc.m409392200.

Winn, R.A., Van Scoyk, M., Hammond, M., Rodriguez, K., Crossno, J.T., Jr., Heasley, L.E., and Nemenoff, R.A. (2006). Antitumorigenic effect of Wnt 7a and Fzd 9 in non-small cell lung cancer cells is mediated through ERK-5-dependent activation of peroxisome proliferator-activated receptor γ. J. Biol. Chem. *281*, 26943–26950. https://doi.org/10.1074/jbc.m604145200.

STAR★METHODS

KEY RESOURCES TABLE

REAGENT or RESOURCE	SOURCE	IDENTIFIER
Antibodies		
ECAD (CD324)	Protein Tech	#RRID: AB_10697811, #20847-1-AP
COX2 (PTGS2)	Protein Tech	#RRID: AB_2881731, #663511lg
Ki67	Abcam	#RRID: AB_443209, #15580
β-actin	BioRad	#RRID: AB_2571580, #MCA5775GA
Precision Protein Streptactin-HRP	BioRad	#1610380
Immun-Star Goat Anti-Mouse (GAM)-HRP Conjugate	BioRad	#1705047
Immun-Star Goat Anti-Rabbit (GAR)-HRP Conjugate	Biorad	#1705046
Protein Precision Ladder	BioRad	#1610375
Chemicals, peptides, and recombinant proteins		
Urethane	Sigma-Aldrich	#943-50g, Lot #WXBC8654V
Iloprost	Cayman Chemicals	#18215
Methyl Acetate	Sigma Aldrich	45999-200ML-F
2-mercaptoethanol	ThermoFisher Scientific	#21985023
10X Tris-Glycine Buffer	BioRad	#1610771
Ponceau S	Fisher Bioreagents	#BP103-10
Non-Fat Dry Milk	LabScientific	#M0841
2X Laemmeli Buffer	BioRad	#1610737
Clarity Western ECL substrate	Biorad	#1705060
Diva Decloaker RTU	Biocare Medical	#DV2004G1
Background Punisher	Biocare medical	#BP974M
2.5% Normal Horse Serum	Vector laboratories	S-2012-50
TransIT-X2 Dynamic Delivery System	Mirus	#MIR6004
GoTaq	Promega	#M7132
Pierce^{TM} RIPA buffer	Thermo Scientific	#89900
Tween-20	Fisher BioReagents	#BP337-500
Sodium Dodecyl Sulfate	Fisher BioReagents	#BP166-500
Tris	Fisher BioReagents	#BP152-1
Glycine Electrophoresis grade	MP Biomedicals, LLC	#808822
RNA Later	Sigma Life Sciences	#R0901
Red Blood Cell Lysing Buffer Hybri-Max	Sigma Life Sciences	#R7757
Critical commercial assays		
Dual-Luciferase Reporter Assay	Promega	#E1960
Pierce^{TM} BCA Assay	Thermo Scientific	#23225
Betazoid Dab Chromagen Kit	Fisher Scientific	#BDB2004L
Sso Advanced Universal SYBR	BioRad	#1725274
High Capacity cDNA Reverse Transcription Kit	Fisher Scientific	#43-688-13
Vectastain Elite ABC anti-mouse/Rabbit RTU HRP immunodetection kit	Novus Biologicals	PK-7200
Experimental models: Cell lines		
HBEC2KT and HBEC3KT	Dr. John Minna	RRID: CVCL_X491, #CRL-4051
A549	ATCC	RRID: CVCL_0023, #CRM-CCL-185

(Continued on next page)

Continued

REAGENT or RESOURCE	SOURCE	IDENTIFIER
Experimental models: Organisms/strains		
FVB/N $Fzd_9^{-/-}$	National Jewish Hospital Regional Mouse Genomics Core Facility	N/A
FVB/N $Pgis^{Tg+}$	University of Colorado	N/A
FVB/N $Pgis^{Tg+}xFzd_9^{-/-}$	Rocky Mountain Regional VA Medical Center Veterinary Medical Unit	N/A
Recombinant DNA		
PPRE	Addgene	RRID: Addgene_1015, #1050
Renilla	Promega	#E2231
Y277S_FZD_9 C-term his tag	Genescript	Lot: U279VGC020-1/Q87680
Oligonucleotides		
Ces1 - Mouse	BioRad	qMmuCID0026391
15pgdh - Mouse	BioRad	qMmuCID0024412
Pparg - Mouse	BioRad	qMmuCID0018821
Crb3- Mouse	BioRad	qMmuCID0008889
Vegf – Mouse	BioRad	qMmuCED0040260
Esr1 – Mouse	BioRad	qMmuCED0044294
Rps18 - Mouse	Biorad	qMmuCED0045430
Vim – Mouse	BioRad	qMmuCED0046651
Ecad - Mouse	BioRad	qMmuCED0044197
Fzd_9 Forward Primer (5'-TGCACATACAGATAGACAAGC-3')	Integrated DNA technologies	#207267468
Fzd_9 Reverse Knockout Primer (5'-GCCAGCCCGGACCTTATTTG-3')	Integrated DNA technologies	#207267470
Fzd_9 Reverse Wildtype Primer (5'-CACTCACTGTAGCTGTCTTCAG-3')	Integrated DNA technologies	#207267469
$Pgis^{Tg}$ Forward Primer (Small Ts) (5'-TGTGAAGGAACCTTACTTCTGTGG-3')	Integrated DNA technologies	#287949701
$Pgis^{Tg}$ Reverse Transgenic Primer (Small Ta) (5'-TGGACAAACCACAACTAGAATGCA-3')	Integrated DNA technologies	#287949702
Software and algorithms		
Graphpad Prism version 9.0.2	Graphad Prism	RRID: SCR_002798, version 9.0.2
Bio-Rad ChemiDoc Imager	BioRad	RRID: SCR_019037
MicroCT- ctAN, CTvol (VGStudio)	Bruker	RRID; SCR_021338, RRID: SCR_017997
CFX Maestro	BioRad	RRID: SCR_018064, #12013758
FlashGel™ System	Lonza	#57062
Other		
RPMI	Thermo Scientific	#11875093
Keratinocyte-SFM	Thermo Scientific	#17005042
Opti-MEM	Thermo Scientific	#31985062
2.2% precast agarose Gels	Lonza	#57032
Mini-PROTEAN Tris/Tricine precast gels	BioRad	#4568094

RESOURCE AVAILABILITY

Lead contact

Further questions should be directed to the lead contact, Meredith Tennis (Meredith.tennis@cuanschutz.edu).

Materials availability

- This study did not generate new or unique reagents.

Data and code availability

- All data reported in this paper will be shared by the lead contact upon request.

- This data does not report original code.

- Any information required to reanalyze the data reported in this paper is available from the lead contact upon request.

EXPERIMENTAL MODEL AND SUBJECT DETAILS

Animals: Mice

$Fzd_9^{-/-}$ mice were developed by the Regional Mouse Genetics Core Facility at National Jewish Health and the University of Colorado. Guide design was done using CRISPR and the Broad Institute sgRNA Design software, both of which have been refined to better identify off target events. Results from each software were compared, and the guide which performed best using both algorithms was chosen. Guide activity was verified by incubating guide RNA and Cas9 protein with a PCR product containing the target sequence and comparing the ratio of cut to uncut PCR product. Zygotes were injected with guide RNA(s), Cas9, and DNA template if appropriate. Zygotes were then transferred into pseudopregnant recipients. F0 pups were genotyped by PCR using primers outside the region to be modified to identify putative positive founders. These mice were then bred to FVB/N wildtype mice. Once germline transmission was established, F1 mice were sequenced to confirm the modification and intercrossed to generate homozygous knockout mice. Two genotyping assays were established to identify $Fzd9^{-/-}$ mice for experiments that include a common forward primer (5-TGCACATACAGATAGACAAGC-3') and separate wildtype reverse primer (5-CACTCACTGTAGCTGTCTTCAG-3') and knockout reverse primer (5-GCCAGCCCGGACCTTATTTG-3'). $Fzd9^{-/-}$ mice were transferred to the Rocky Mountain Regional Veterans Affairs Medical Veterinary Care Unit (RMRVAMC VMU) and animals for experiments were generated by breeding $Fzd9^{-/-}$ males with $Fzd9^{-/-}$ females to generate 100% knockout litters.

FVBN prostacyclin synthase transgenic ($Pgis^{Tg}$) mice were developed using a construct containing the human surfactant protein-C (SP-C) promoter and full-length rat $Pgis$ cDNA (Nemenoff et al., 2008). $Pgis^{Tg}$ heterozygote mice are bred with FVB/N wildtype mice to generate the heterozygotes used in experiments. To generate $Pgis^{Tg}$ x$Fzd_9^{-/-}$ mice, $PGIS^{Tg}$ (het) mice were bred with $Fzd_9^{-/-}$ mice, resulting in 50% $Pgis^{Tg}$ (het)x$Fzd9^{-/+}$ mice. $Pgis^{Tg}$ (het)x$Fzd9^{-/+}$ mice were then crossed, resulting in 50% $Pgis^{Tg}$ (het) x$Fzd_9^{-/-}$. Subsequent $Pgis^{Tg}$ (het)x$Fzd_9^{-/-}$ animals were generated by breeding $Pgis^{Tg}$ (het)x$Fzd_9^{-/-}$ mice with $Fzd_9^{-/-}$ mice, for 50% $Pgis^{Tg}$ (het)x$Fzd_9^{-/-}$ litters. All animals for experiments were bred at the RVRVAMC VMU. All procedures were performed with IACUC approved protocols at the RVRMAF VMU.

Mouse genotyping

To confirm continued genotypes in mice used for experiments, genomic DNA was extracted from ear clips of each mouse with a DNeasy Blood & Tissue kit (Qiagen). The DNA was amplified by RT-PCR with forward and reverse DNA primers and GoTaq Green Master mix (Promega) on a CFX96 Touch (Biorad). To confirm $Fzd9^{-/-}$ genotype, a knockout gel and wildtype gel were run. The same forward primer was used for both reactions (5'-TGCACATACAGATAGACAAGC-3'), while the knockout reverse primer (5'-GCCAGCCCGGACCTTATTTG-3') identified a sequence left by the CRISPR manipulation and the wildtype reverse primer (5'-CACTCACTGTAGCTGTCTTCAG-3') identified WT $Fzd9$. $Pgis^{Tg}$ genotyping used the published protocol with forward primer (5'-TGGACAAACCACAACTAGAAT-3') and reverse primer (5'-TGTGAAGGAACCTTACTTCTGTGG-3') (Nemenoff et al., 2008). PCR product was analyzed by electrophoresis in precast 2.2% agarose gels at 275V (Lonza). Gels were imaged with the FlashGel™ Dock and the FlashGel™ camera using the FlashGel™ Camera and Capture software.

$Fzd_9^{-/-}$ inhaled iloprost *in vivo* study

Male and female mice (8 weeks old) were housed in a pathogen-free facility in the RMRVAMC VMU in four groups: wild type saline, wild type urethane, $Fzd_9^{-/-}$ saline, and $Fzd_9^{-/-}$ urethane. Nine mice were included in each wild type group and 12 in each $Fzd_9^{-/-}$ group. Mice were injected IP with 100 μL of 1 mg urethane/g body weight dissolved in the 0.9% saline vehicle or 100ul saline vehicle only (Fritz et al., 2014). Mice were weighed daily for 7 days after urethane injection and weekly for the remainder of the experiment. Nine weeks after urethane exposure, iloprost (Cayman Chemicals) or the saline vehicle was administered intranasally at a dose of 5 μg/mouse/100 μL (50 μL per nare with a P200 pipette), five days/week for 6 weeks (Figure 1A). Mice were anesthetized with isofluorane, half the iloprost was delivered to one nare, followed by a pause to observe inhalation, and then the second half of the dose was delivered to the second nare (Lammi et al., 2016). This iloprost treatment regimen was used because small pre-malignant adenomas are detectable in mice after 6 weeks of urethane exposure and mice can tolerate iloprost intranasal treatment (Lammi et al., 2016; Fritz et al., 2014). Following the last iloprost treatment at 15 weeks post urethane, mice were sacrificed by a lethal dose of Fatal Plus. Serum was collected by cardiac puncture. Lesions were dissected from surrounding lung tissue and diameters measured with digital calipers. Surrounding lung tissue was saved for RNA extraction. Studies were carried out in accordance with the recommendations in the NIH Guide for the Care and Use of Laboratory Animals and were approved by the RMRVAMC Animal Care and Use Committee.

$Pgis^{Tg}$ x $Fzd_9^{-/-}$ urethane *in vivo* study

Females and males (8 weeks old) were housed in a pathogen-free facility in the RMRVAMC VMU in six groups: wild type saline, wild type urethane, $Pgis^{Tg}$ saline, $Pgis^{Tg}$ urethane, $Pgis^{Tg}xFzd_9^{-/-}$ saline, and $Pgis^{Tg}x Fzd_9^{-/-}$ urethane. The $Pgis$ transgene leads to increased levels of prostacyclin and development of the model has been published (Keith et al., 2002). Mice received an IP injection of 100uL of 1 mg urethane/g body weight dissolved in the 0.9% saline vehicle or saline vehicle alone. Mice were weighted daily for 7 days after urethane injection and weekly for the remainder of the experiment. 16 weeks after the urethane injection, the mice were sacrificed by a lethal dose of Fatal Plus. Lesions were dissected from surrounding lung tissue using a dissecting microscope and diameter measured with digital calipers. Studies were carried out in accordance with the recommendations in the NIH Guide for the Care and Use of Laboratory Animals and were approved by the RMRVAMC Animal Care and Use Committee.

Cells

Non-transformed human bronchial epithelial cells (HBEC3KT (male) and HBEC2KT (female)) (gifts from the lab of Dr. John Minna, UT Southwestern) were cultured in Keratinocyte Serum Free Medium (GIBCO). All HBEC cell cultures were grown and handled in a dedicated incubator. A549 human lung cancer cell line (male, purchased from the Cell Technologies shared resource at the University of Colorado Cancer Center), was cultured in RPMI (GIBCO) with 10% fetal bovine serum. 293T human embryonic kidney cell line (ATCC) was cultured in DMEM (GIBCO) with 10% fetal bovine serum. All cell lines were carried at 37°C in a humidified 5% CO_2 incubator and passaged twice per week. All *in vitro* studies were approved by the University of Colorado Institutional Biosafety Committee.

METHOD DETAILS

MicroCT imaging

Three mice/group were imaged immediately before harvest. Mice were anesthetized with isoflurane and imaged in Bruker 1276 Skyscan microCT by placing mice prone in a heated mouse bed with breathing cone and supplied with oxygen and isoflurane to maintain anesthesia. Image parameters were as follows: X-ray tube voltage of 70 kV, current of 200 μA, pixel size of 40.79 μm, exposure time of 167 ms with 0.5 mm aluminum filter and 0.7 rotation stepping. Using the computer program CTan by Bruker, the CT scan was turned into a binary image. The threshold for what was considered tumor and vessel, which are approximately the same density vs what is considered aerated lung tissue is chosen by the person performing the data analysis. This threshold is chosen based on closely matching the binary image of the scan to the actual scan. The same threshold was then applied to each scan. With CTan, an automatic series of computer operations separates the aerated lung tissue from the rest of the mouse. The lungs are then selected as a region of interest and the tumors and vessels are selected from this lung region. A 3D reconstruction was then made of the vessels and tumors and tumors were identified manually and differentiated from vessels. Vessels were removed through a combination of manual deletion and automatic computer

operations. Data analysis was then performed to obtain tumor count and tumor volume. The 3D models were then generated in CTan and visualized in the program CTvol, also by Bruker.

Reverse transcriptase-quantitative PCR

Mouse lung tissue and lesions were collected in RNA Later (Qiagen) at the time of harvest. qPCR Prime PCR Assays (Bio-Rad) for mouse included: *Crb3, Vegf, Esr1, 15pgdh, Ecad, Ces1, Pparg, Vim,* and *Rps18*. qPCR was conducted using standard protocol for Sso Advanced SYBR Green Master Mix (Bio-Rad) on a CFX96 Touch (Bio-Rad).

Western blots

Protein was extracted using Pierce RIPA buffer (Thermo Scientific) and protease inhibitor (Thermo Scientific). The samples were quantified by BCA assay (Thermo Scientific). 20ug of protein was mixed with 2X laemmeli buffer and BME for a 1:1 sample, denatured at 56°C for five minutes and electrophoresed and transferred with a molecular marker according to the manufacturer's protocol (Mini-Protean Tetra Cell, BioRad). Membranes were stained with 0.1% Ponceau S to confirm sufficient protein transfer. The membrane was blocked in 10 mL of 5% Non-Fat dry milk in 1X TBS-T for 1 hour, followed by three 15-minute washes with 1X TBS-T. Blots were incubated in primary antibody (COX2 1:500 Protein tech #663511Ig, ECAD 1:3,000 Protein Tech #20874-1-AP) overnight at 4°C. Membranes washed and incubated in diluted 1:5,000 secondary anti-rabbit IgG antibody (BioRad) and 1:5000 StrepTactin HRP conjugate (Biorad) for 1 hour. Membranes were washed and exposed to 2 mL of Clarity Western ECL substrate (Biorad) for five minutes. Images were captured and quantified with a ChemiDoc imager (BioRad). To confirm protein loading, the membrane was stripped, rinsed, blocked, and probed for B-actin (Biorad #MCA5775GA).

Immunohistochemistry

5 μm lung sections from urethane, iloprost, and saline groups were deparaffinized, blocked with 0.3% hydrogen peroxide, and antigen retrieval performed in boiling Diva Decloaker (Biocare Medical, DV2004G1) under pressure for 5 minutes. Sections were blocked with Background Punisher (Biocare Medical BP974M) and 2.5% Normal Horse serum (Vector Labs S-2012-50). Sections were incubated in Ki67 primary Ab (1:2000 dilution, Abcam 15580) for 1 hour at room temperature, followed by anti-rabbit universal antibody for 30 minutes and ABC reagent for 30 minutes at room temperature (Vector Laboratories PK-7200). Ki67+ nuclei were detected using Betazoid DAB chromagen kit (Vector Laboratories BDB2004). Tumor area was measured and Ki67-positive nuclei/mm^2 were counted in each tumor. Replicate blinded counts were conducted. The Ki67+ nuclei/mm^2 tumor area for each tumor was averaged by group (Dwyer-Nield et al., 2017). H&E stains were done on 5 μm lung sections from urethane, iloprost, and saline groups and were used to confirm adenoma presence and structure.

Serum PPARG activity assay

Serum was collected by intracardiac puncture immediately after euthanizing each mouse. 293t cells were seeded at 2,000 cells/well in a 96 well plate. After twenty-four hours, the cells were transfected with 45 ng PPARG response element firefly luciferase (PPRE was a gift from Bruce Spiegelman; Addgene plasmid #1015) and 5 ng renilla control reporter vector (Promega) using TransiIT-X2 transfection reagent (Mirus Bio) and Opti-MEM media (Thermo Fisher) per the manufacturer's protocol. Cells were treated with 10ul mouse serum at 24 hours and 48 hours post transfection (Edwards et al., 2019). Serum treatments were conducted in triplicate and included empty and mock transfection controls. Luciferase activity was measured after 48 hours using the Dual-Luciferase Reporter assay kit (Promega) on the Glomax instrument (Promega).

In silico binding prediction

The homology model of human FZD9 was generated using Biovia Discovery Studio 2018 (Biovia, Inc) using the structure of the human smoothened receptor as a template (Wang et al., 2013). YASARA Structure 19.1 (Yasara Biosciences GmbH, Vienna, Austria) was used to evaluate the quality of the resulting homology models, which were subjected to 1 ns of explicit solvent-based MD simulation utilizing the YASARA2 force field (Krieger et al., 2002, 2009). The snapshots of the MD simulation (taken every 25 ps) were evaluated using the WHAT_IF and WHAT_CHECK structure validation tools to quantitatively evaluate the overall quality of each predicted structure (Hooft et al., 1996; Vriend, 1990). The highest scoring structure snapshot had a Z-score of −0.15, indicating the homology model had a high degree of compatibility with the protein sequence and was of similar quality to that of the average of ∼30,000 high-resolution crystal structures

contained in the Protein Data Bank. This structure was used for the subsequent docking studies. The binding mode of Iloprost was predicted using the flexible docking protocol within Discovery Studio coupled with binding energy analysis utilizing the Generalized Born with Simple Switching (GBSW) implicit solvent model (Koska et al., 2008; Feig et al., 2004). The binding site sphere was set large enough to encompass the vast majority of the solvent accessible surface of the protein. The final ranking of the docked poses was performed via consensus scoring, combining the predicted binding energy with overall number of favorable intermolecular contacts and the Jain,[29] PLP2,[30] and Ludi3[31] scoring functions. Figures were rendered using Lightwave 2018 (Lightwave3D Group) and Photoshop CC 2018 (Adobe Systems, Inc.).

Mutant plasmid transfections

A human FZD_9 mutant plasmid with a serine substitution for tyrosine at amino acid 277 (Y277S) was generated by GenScript (Piscataway, NJ) using site-directed mutagenesis. A549 and HBEC cells were transfected with 45 ng PPRE-luciferase, 5 ng renilla control reporter vector, plasmid control vector, and/or FZD_9 Y277S plasmid using TransIT-X2 transfection reagent and Opti-MEM media per the manufacturer's protocol. Cells were treated at 24 and 48 hours with 10uM of Iloprost or methyl acetate vehicle and analyzed for PPRE luciferase activity as described above.

QUANTIFICATION AND STATISTICAL ANALYSIS

$Fzd_9{}^{-/-}$ adenoma counts

The number of adenomas per mouse in urethane exposed wildtype or $Fzd_9{}^{-/-}$ mice treated with iloprost or a saline control were averaged for each group (Figure 1C). Statistical analysis one-way ANOVA with Tukey post-hoc analysis was conducted using GraphPad Prism (RRID: SCR_002798, version 9.0.2). *p < 0.05 Error bars represent SEM for each group.

Mice

WUS: n = 7

WUI: n = 10

FUS: n = 10

FUI: n = 9

$Pgis^{Tg}$ x $Fzd_9{}^{-/-}$ adenoma counts

The number of adenomas in urethane treated wildtype, $Pgis^{Tg}$, and $Pgis^{Tg}$ x $Fzd_9{}^{-/-}$ were averaged for each group (Figure 2B). Statistical analysis using a one-way ANOVA with Tukey post-hoc analysis was conducted using GraphPad Prism. *p < 0.05 Error bars represent SEM for each group.

Mice

WT: n = 4

$Pgis^{Tg}$: n = 4

$Pgis^{Tg}xFzd_9{}^{-/-}$: n = 25

Adenoma diameter measurements

The diameter of each adenoma was measured with a digital caliper (Figures 1D and 2C). One-way ANOVAs with Tukey post-hoc analysis were performed in Graphpad Prism to determine statistical significance between groups in each experiment. *p < 0.05 Error bars represent SEM for each group.

Inhaled Iloprost $Fzd_9{}^{-/-}$ Study:

WUS: n = 23

WUI: n = 23

FUS: n = 44

FUI: n = 48

Pgis^{Tg}xFzd$_9^{-/-}$ Study:

WT: n = 17

Pgis^{Tg}: n=4

Pgis^{Tg}xFzd$_9^{-/-}$: n = 19

Average weight change in mouse studies

The weight change per mouse was measured weekly for each group until the end of the study (Figures 1B and 2A). The weight changes for each mouse were averaged by group to show the average weight change every week per group. One-way ANOVAs with Tukey pos-hoc analysis in Graph-Pad Prism was performed to determine significance between groups. *p < 0.05 Error bars represent SEM.

Mice.

Inhaled Iloprost *Fzd$_9^{-/-}$* Study:

WUS: n = 9

WUI: n = 9

FUS: n = 12

FUI: n = 14

Pgis^{Tg}xFzd9$^{-/-}$ Study:

WT: n = 9

Pgis^{Tg}: n = 9

Pgis^{Tg}x Fzd$_9^{-/-}$: n = 29

Reverse transcriptase-quantitative PCR

All gene expression data was normalized to the reference gene *Rps18* and fold changes were calculated using the $2^{-\Delta\Delta Ct}$ method. PCR analysis was conducted in triplicate and statistical analysis was done by Student's t-test comparing the urethane/iloprost mice to their genotype urethane/saline control (Figures 3A and 3B). *p < 0.05 For extraction of adenoma RNA, all lesions dissected from an individual mouse were pooled. Error bars represent SEM.

Adenoma qPCR:

WUI: n = 5

FUI: n = 8

Lung qPCR

WUI: n = 12

FUI: n = 8

Western Blot quantitative analysis

Quantitative analysis was performed by creating a ratio between the band intensity for the protein of interest and the sample's corresponding β-actin band intensity. Blots were repeated in duplicate and band intensity ratios were averaged (Figure 3D). A one-way ANOVA with Tukey post-hoc analysis in GraphPad Prism was used to measure significance. $*p < 0.05$ Error bars represent SEM.

Ki67 proliferative index

Lesion area was measured and Ki67-positive nuclei/mm^2 were counted in each lesion. Replicate blinded counts were conducted. The Ki67+ nuclei/mm^2 lesion area was averaged by group (Dwyer-Nield et al., 2017). A one-way ANOVA with Tukey post-hoc analysis in GraphPad Prism was used to measure significance (Figure 1E). $*p < 0.05$Error bars represent SEM.

Adenomas stained

WUS: n = 4

WUI: n = 1

FUS: n = 3

FUI: n = 4

Serum PPARG activity assay

PPRE-luciferase activity was normalized to renilla activity and analyzed relative to the wild type saline group. Each serum sample was performed in triplicate and averaged. N = 3 for each sample group. Significance was assessed by one-way ANOVA with Tukey post-hoc analysis in GraphPad Prism (Figure 4). $*p < 0.05$ Error bars represent SEM.

Site directed mutagenesis

PPRE-luciferase activity was normalized to renilla activity and analyzed relative to empty controls. Each transfection was performed with technical triplicates and averaged. N = 3 for each sample group. Significance was assessed by one-way ANOVA with Tukey post-hoc analysis in GraphPad Prism (Figures S2C and S2D). $*p < 0.05$ Error bars represent SEM.